# Interferometric *in situ* alignment for UV-based nanoimprint

A. Fuchs,[a] B. Vratzov, T. Wahlbrink, Y. Georgiev, and H. Kurz
*Advanced Microelectronic Center Aachen—AMICA, AMO GmbH, Huyskensweg 25, D-52074 Aachen, Germany*

(Received 2 June 2004; accepted 30 August 2004; published 10 December 2004)

A high precision alignment concept is evaluated for suitability in UV-based nanoimprint lithography. Through three consecutive alignment steps an overlay accuracy of 50 nm is obtained with ample room for further improvements. © *2004 American Vacuum Society.* [DOI: 10.1116/1.1808735]

## I. INTRODUCTION

Nanoimprint lithography offers great potential in accuracy, high resolution, and reproducibility.[1–3] Overlay with alignment precision in the range of the resolution is mandatory for a large number of applications. Specific process details of UV nanoimprint lithography (UV-NIL)[4] offer three main advantages to reach the overlay accuracy required. First, the transparent imprint molds allow one to adopt alignment techniques developed for optical or x-ray lithography. Second, the absence of thermal cycles in UV-NIL enhances the overlay accuracy principally and is favorable for optical interferometric techniques. Third, prior to UV curing the imprint resist remains in a state of low viscosity, allowing fine alignment in contact mode. Alignment errors that may occur during lowering of the imprint mold to the substrate surface and the imprint into the resist can be corrected within certain margins. The extremely small gap as well as the strong parallelism between mold and resist surface enhances signal quality and the achievable resolution. In this contribution, we would like to present some details of interferometric alignment technique previously developed for x-ray lithography.[5,6] The theoretical overlay accuracies down to the sub-20 nm regime[7] appear as an attractive solution for UV-NIL.

## II. ALIGNMENT METHOD

The alignment scheme is sketched in Fig. 1. Gratings with a constant period $g$ are fabricated on the surface of the imprint mold and of the substrate. They are brought in near contact separated only by the thin residual resist thickness underneath the imprint mold features. A laser beam incident perpendicular to the surface is diffracted from both gratings in two orders. The zero-order beam (0) from the mold grating is diffracted on the wafer grating ($\pm 1$) and interferes with the $\pm 1$ order diffraction from the mold grating reflected from the substrate (0). Under normal incidence, the $n$th-order diffraction angles $\phi$ are defined by $g \sin(\phi) = n\lambda$, with the laser wavelength $\lambda$.

The interferometric alignment technique is based on the phase shift $\Delta\varphi$ in the diffracted orders originating from a displacement $\Delta x$ orthogonal to its lines under an incident beam. The phase shift $\Delta\varphi$ in the firstorder diffraction is given by $g\Delta\varphi = 2\pi\Delta x$. Interference of these beams to diffraction beams from a stationary grating leads to a change in intensity of the beams in the $\pm 1$ diffractions, which can be read out sensitively by photodetectors. If the detectors show equal intensities, the gratings are oriented highly symmetrically, corresponding to perfect alignment. Since the intensity in the diffracted beams is a periodic function of the relative displacement $\Delta x$, this interferometric alignment technique is only possible in a range $\Delta x < g/2$.

## III. EXPERIMENTAL PROCEDURE

For alignment studies in UV-nanoimprint, two single-crystal $SiO_2$ imprint molds with a diameter of 1 in. have been fabricated. The mold patterns consist of crossbar alignment marks for coarse alignment placed in the edges of the imprint area and an interference grating with a period of 1 $\mu$m for fine alignment. The patterns, defined by electron-beam lithography, were transferred via reactive ion etching (RIE) into the mold substrate. The first mold is used to define a primary pattern onto the silicon substrates (layer A) by UV nanoimprint. Substrates were spin coated with imprint resists, consisting of a mixture of 3-methacryloxypropyltrimethoxysilan and 2-isopropyloxyethanol to a thickness of 190 nm. Next, the imprint mold was pressed into the liquid resist under a pressure of 300 mbar and cured under UV light. The final pattern was then transferred to a depth of 110 nm into the silicon substrate using a $SF_6/O_2$ RIE process. The remaining resist was removed in $H_2SO_4$ and HF acid. These layer A substrates were coated with the imprint resist via spinning and the second mold pattern (layer B) was subsequently applied for a second imprint cycle aligned to layer A.

The alignment experiments were performed with a setup illustrated in Fig. 2. Carrying the layer A substrate, a wafer alignment table equipped with a stage for $x$, $y$, and $\theta z$ scans is applied ($\Delta x_{\min} = \Delta y_{\min} = 50$ nm, $\Delta\theta z_{\min} = 6$ $\mu$rad). For fine alignment, the layer B mold is mounted to a high precision piezostage with $x$, $y$, and $\theta z$ scans ($\Delta x_{\min} = \Delta y_{\min} < 10$ nm, $\theta z_{\min} = 30$ nrad). The piezostage can be moved in the $z$ axis to the base plate with pressure for the imprint procedure. An optical microscope is used for coarse alignment via optical marks. The interference alignment is performed with a HeNe laser (632.5 nm) under normal inci-

[a]Electronic mail: fuchs@amo.de

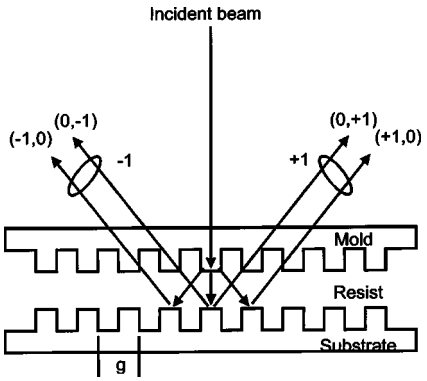


FIG. 1. Sketch of the interferometric alignment: An incident laser beam is diffracted from the mold and the wafer grating. ±1 diffraction orders from the mold grating are reflected (0) on the wafer and interfere with the ±1 diffraction orders from the wafer grating.

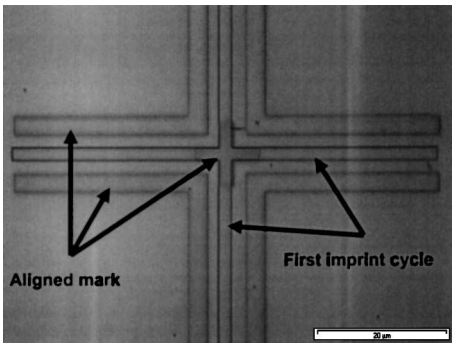


FIG. 3. Marks used for coarse alignment; the middle crossbar has a width of 2 $\mu$m and is patterned in the first imprint cycle. Outer L-bars are oriented to the prepatterned substrate via optical microscope.

dence to the mold and the wafer grating. A grating period of 1 $\mu$m has been chosen with a diffraction angle relative to the incident beam of 39.3°. Two photodetectors monitor the intensities in the ±1 diffraction orders.

Alignment is performed in three steps. First, the layer B mold and the resist-coated layer A silicon substrate are brought to a close distance (5 $\mu$m), where the marks on both layers become observable. Since the mold pattern and the resist surface are not yet in contact, large lateral movements against each other are possible. Next, the mold is lowered and comes in contact with the liquid imprint resist surface under pressure. In this shape, where the imprint resist fills the mold's features, the following alignment errors caused by vertical movement of the mold and its contact to the resist surface have to be considered to achieve alignment accuracies <50 nm. First, guidance errors occur if the *z*-direction bearings have tolerances >1% of the travel range. Second, placement errors arise from vibrations coupled from the imprint tool environment. Third, errors caused by the tendency of the mold to move laterally when brought in contact with the resist surface. These errors can only be reduced by constructing an ultrarigid mold holder. However, on the other hand, the imprint mold holder needs flexibility for compensation of surface wedges.

For that reason, a second coarse alignment step, the readjustment in contact after filling up of the imprint resist, is indispensable for alignment in the sub-500 nm regime ($g/2$ for interferometric alignment). As both marks are now nearly in the same focal plane, the visibility of the marks is enhanced. However, the contrast of the alignment marks drops rapidly after filling with the imprint resist due to the smaller refractive index contrast between the mold substrate and the resist compared to air. Therefore, specific measures to enhance the contrast of the optical microscope have to be taken. Lateral movements after contact of the mold features within the resist should be limited to approximately 20 $\mu$m. For larger distances, the mold tends to form a wedge and a constant residual resist layer is no longer achievable. Furthermore, pattern quality degrades because the resist refilling of the features is not complete. Therefore, permanent online readjustment between the mold and the substrate during the *z* movement of the mold and the filling of the mold features is required to achieve maximum alignment accuracies in the range of optical alignment marks.

An optical micrograph of aligned marks is shown in Fig. 3. The 2 $\mu$m-wide large crossbar in the middle has been defined in the first imprint cycle and transferred into the silicon sample. The large outer L-bars and the small center cross are aligned and imprinted in a second imprint procedure. The image illustrates that alignment accuracy down to half of the interferometric grating pitch (sub-500 nm) has been achieved using these bars after the optical alignment procedure. However, enhancement of the accuracy is difficult to achieve due

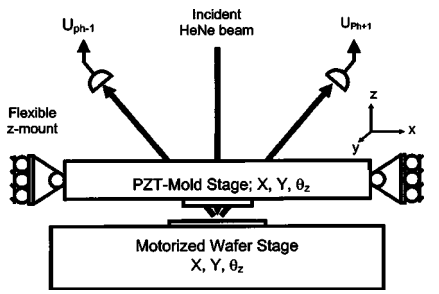


FIG. 2. Interferometric setup; wafer stage consists of dc motors for coarse alignment in *x*, *y*, and $\theta z$; piezo-driven mold stage for high resolution *x*, *y*, and $\theta z$ scans.

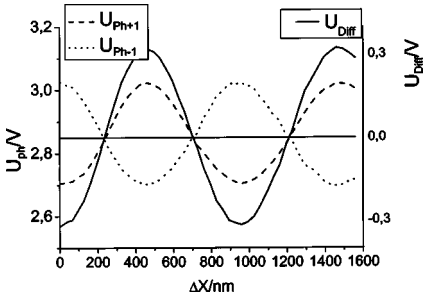


FIG. 4. Plot of signal intensities measured in the ±1 diffraction beams ($U_{Ph+1}$, $U_{Ph-1}$) and their difference signal ($U_{Diff}$ solid line) vs displacement between mold and substrate.

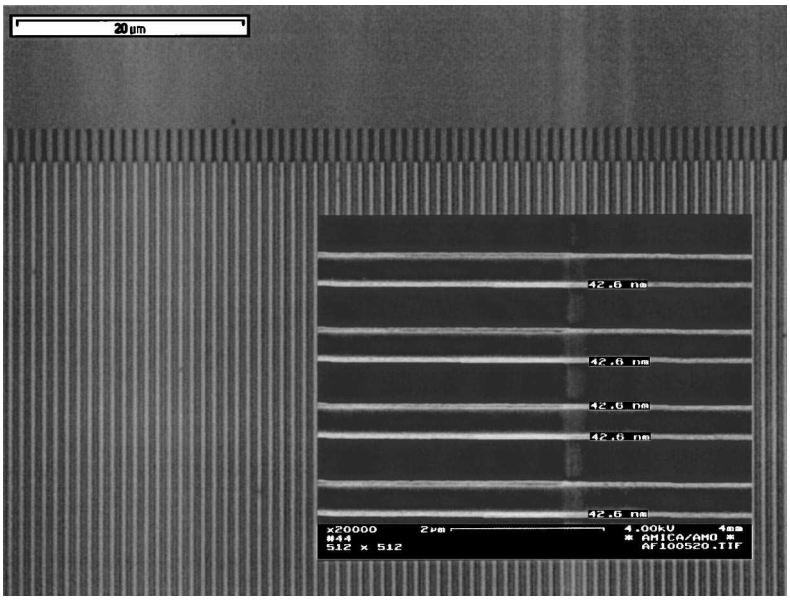


FIG. 5. Optical microscope and SEM image of two alignment gratings oriented to each other via interferometric alignment.

to technical limitations of the optics of the microscope; for example, working distance, resolution, and depth of field.

To improve the overlay accuracy, the alignment technique is changed from optical microscopy to interferometric alignment in the next step. A HeNe laser beam is directed at normal incident onto the center of the alignment gratings. The diffraction signals are fed into the photodetectors and their signal is further processed. The signals are calibrated and offset compensated. Finally, the mold and the substrate are moved until both signals are balanced, indicating a highly symmetric position of the grating. After the third alignment procedure step, the resist is cured through the mold's backside and the mold is detached.

## IV. RESULTS AND DISCUSSION

In Fig. 4 the intensities of the ±1 diffracted beams are plotted versus the lateral shift between the mold and the layer A substrate ($\Delta x$). Here, the mold and the substrate are moved against each other perpendicular to the lines of the interference grating over a length of 1600 nm. The difference signal is plotted by the solid line in the graph. At $\Delta x = 250$nm the slope of the difference curve is determined to be 2.4 mV/nm. This lateral displacement sensitivity allows one to reach nanoscale accuracy.

The results of final interferometric alignment are shown in Fig. 5 where longer grating lines prepatterned in the silicon substrate are aligned to the shorter ones. The magnified Scanning electron microscope (SEM) image in Fig. 5 illustrates these lines 90° rotated while the ends of the shorter layer B lines are barely discernible. SEM analysis identifies an alignment error between the lines of the interference gratings of less than 50 nm. However, charging hampers a more accurate error measurement.

A second method for overlay detection has been applied using vernier scales. Here, a grating period of 200 nm for the first imprint cycle and of 190 nm for the second one results in a vernier pitch of 10 nm. They have been placed next to the grating and can be seen in Fig. 6. By counting the scale periods from the middle until both lines match perfectly, the alignment error can be determinend by multiplying the counts and the vernier pitch. For Fig. 6, an alignment error of 40–50 nm can be deduced.

## V. CONCLUSION

By employing a three-step alignment process of two consecutive alignment techniques, the overlay accuracy in UV-based nanoimprint lithography could be improved to 50 nm. Alignment in the 20 nm regime appears feasible if potential improvements in the optical read out and displacement detection are exploited.

## ACKNOWLEDGMENTS

This work is partially supported by the Bundesministerium für Forschung und Bildung (BMB+F), Contract Num-

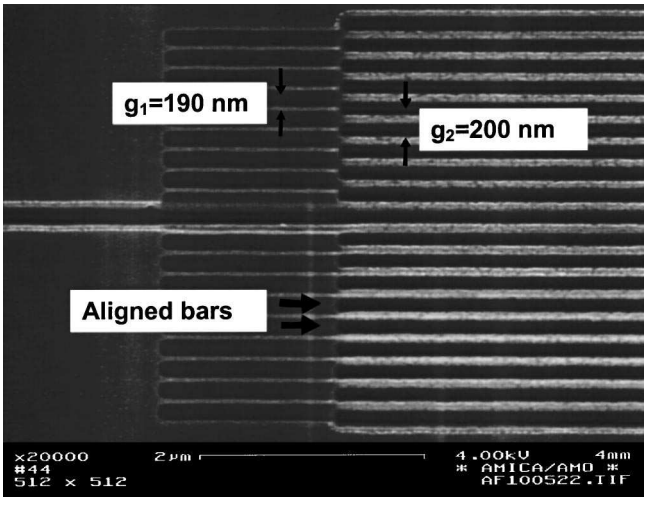


FIG. 6. SEM image of a vernier scale used for displacement detection.

ber 13N 8399. The authors are also grateful to M. Bender and U. Plachetka from AMO GmbH and to P. Haring from the Institute of Semiconductors, RWTH-Aachen, Germany.

[1]S. Y. Chou, P. R. Krauss, and P. J. Renstrom, Appl. Phys. Lett. **67**, 3114 (1995).
[2]J. Haisma, M. Verheijen, K. v. d. Heuvel, and J. v. d. Berg, J. Vac. Sci. Technol. B **14**, 4124 (1996).
[3]M. Colburn, A. Grot, M. Amistoso, B. J. Choi, T. Bailey, J. Ekerdt, S. V. Sreenivasan, J. Hollenhorst, and C. G. Willson, SPIE's 25th International Symposium on Microlithography: Emerging Lithography Technologies III, Santa Clara, CA, 2000.
[4]B. Vratzov, A. Fuchs, M. Lemme, W. Henschel, and H. Kurz, J. Vac. Sci. Technol. B **21**, 2760 (2003).
[5]D. C. Flanders and H. I. Smith, Appl. Phys. Lett. **31**, 426 (1977).
[6]D. L. White and O. R. Wood, J. Vac. Sci. Technol. B **18**, 3552 (2000).
[7]S. Austin, H. I. Smith, and D. C. Flanders, J. Vac. Sci. Technol. B **18**, 3552 (2000).